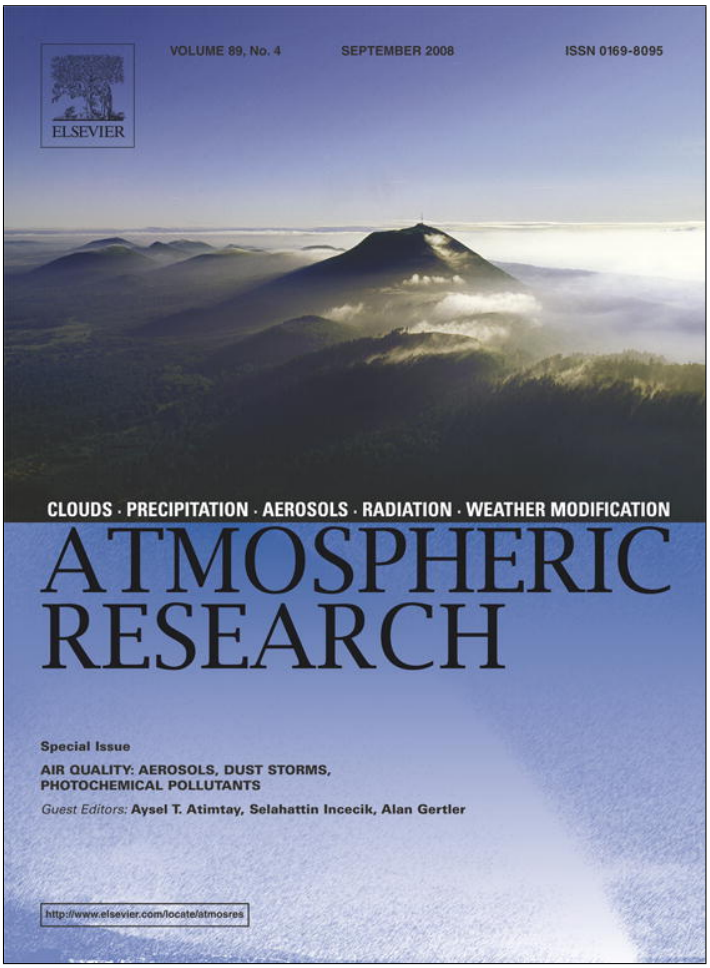

Atmospheric Research 89 (2008) 365–373

Contents lists available at ScienceDirect

Atmospheric Research

journal homepage: www.elsevier.com/locate/atmos

Atmospheric effects on winter SO_2 pollution in Lanzhou, China

Peter C. Chu [a,*], Yuchun Chen [b], Shihua Lu [b]

[a] Naval Ocean-Atmospheric Prediction Laboratory, Naval Postgraduate School, Monterey, California, USA
[b] Cold and Arid Regions Environmental and Engineering Research Institute, Chinese Academy of Sciences, Lanzhou, China

ARTICLE INFO

Keywords:
SO_2 concentration
RAMS-HYPACT
Air pollution index
Stable stratification
Inversion

ABSTRACT

Lanzhou is one of the most polluted cities in China. Sulfur dioxide (SO_2) concentrations have shown evident seasonal variability. Pollution was generally within the second-level criterion (<0.15 mg m^{-3}) in spring, summer, and fall but was much higher than the second-level criterion and sometimes reaches mid-level pollution (API$>$200) in winter. Meteorological conditions (low winds, stable stratification) were found to be important for SO_2 pollution. Observational and modeling studies conducted in the present study showed a close connection between static stability and SO_2 pollution in Lanzhou, China, during winter.

1. Introduction

Lanzhou is located in a long (40 km), narrow (2–8 km), northwest–southeast-oriented valley basin (elevation approximately 1500 m) with the Tibetan Plateau in the west, Baita Mountain (elevation above 1700 m) in the north, and Gaolan Mountain (elevation above 1900 m) in the south (Fig. 1a). The aspect ratio of the valley (depth versus width) is around 0.07. Lanzhou contains four districts (Fig. 1b): Chengguan, Qilihe, Xigu, and Anning. Chengguan (District I), located in the eastern valley, is the metropolitan area and includes government, commerce, cultural, and residential elements. Xigu (District III), located in the western valley, is the large, heavy industrial area. Qilihe (District II), located in the middle portion of the valley, and Anning (District IV), located in the north-middle portion of the valley, are a mix of residential areas, small factories, and farming (vegetables) areas.

Annual and daily mean air quality standards for urban areas established by the State Environmental Protection Agency (SEPA) are used as the air quality criteria. In Lanzhou, the second-level standard is applied to commercial and residential regions, and the third-level standard is applied to industrial regions. For the pollutant sulfur dioxide (SO_2), the annual mean second-level and third-level criteria are 0.06 and 0.10 mg m^{-3}, respectively. The daily mean second-level and third-level criteria for SO_2 are 0.15 and 0.25 mg m^{-3}, respectively (Table 1). When SO_2 concentrations are higher than air quality criterion, the local SEPA will give the air pollution alert.

Lanzhou is an industrial city famous for petrol chemistry, metallurgy, and mechanical manufacturing. Fig. 2 shows the spatial distribution of the annual SO_2 emission rate per square kilometer (10^3 kg km^{-2} yr^{-1}) in 2000. Emission rates are high in District I (commercial and residential) and District III (industrial) (indicated with "H" in Fig. 2). The total SO_2 emission from Lanzhou was 4.43×10^7 kg with 2.15×10^7 kg from industrial sources (Jiang et al., 2001).

Special topographic features of the Lanzhou metropolitan area block air streams due to large frictional forces and cause weak winds. In the winter, calm winds occur nearly 80% of the time. In the evening and occasionally in the daytime, low-level inversions inhibit turbulent diffusion. Lanzhou is one of the most polluted cities in China (Fig. 1c). Shang et al. (2001) show significant correlation between static stability and SO_2 concentrations. An air quality monitoring system has been established in Lanzhou with a sufficient number of sampling stations. This monitoring system was the part of the study entitled, "Air Pollution and Control in Lanzhou" (APCL), which was supported jointly by the Gansu Province and Chinese Academy of Sciences and carried out from 1999–2001.

In the present study, SO_2 pollution in the Lanzhou metropolitan area was analyzed. A coupled Regional Atmospheric Modeling System (RAMS) and Hybrid Particle and

* Corresponding author. Tel.: +1 831 656 3688; fax: +1 831 656 3686.
E-mail address: pcchu@nps.edu (P.C. Chu).
URL: http://faculty.nps.edu/pcchu/ (P.C. Chu).

0169-8095/$ – see front matter © 2008 Elsevier B.V. All rights reserved.
doi:10.1016/j.atmosres.2008.03.008

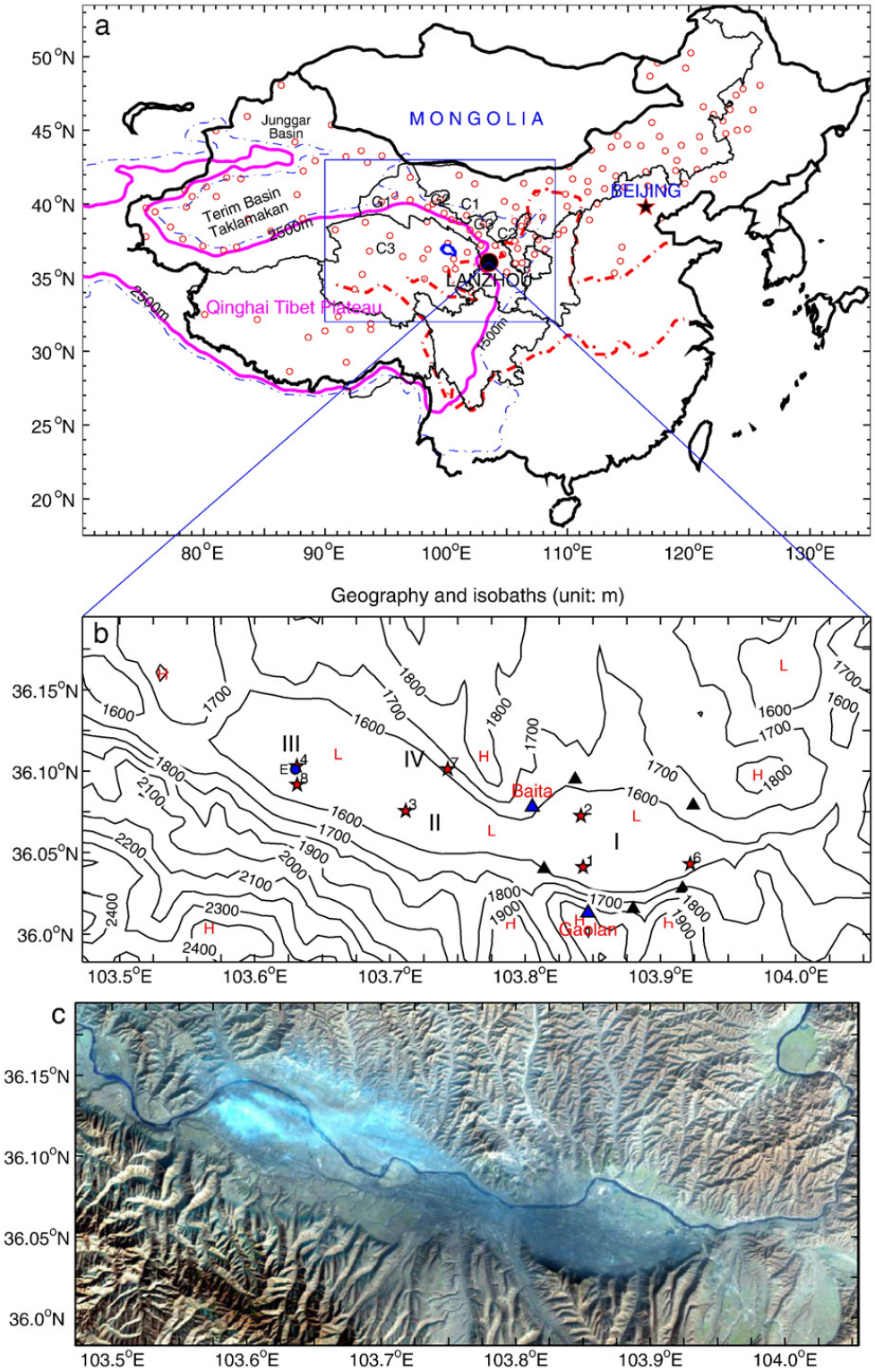

Fig. 1. Lanzhou (a) geography, (b) topography, and (c) LANDSAT-TM imagery representing air pollution on January 3, 2001.

Concentration Transport Model (HYPACT) (Tripoli and Cotton, 1982; Pielke, et. al., 1992) were used to simulate diffusion and transport of SO_2. Objectives of the study were to detect temporal and spatial SO_2 variability, evaluate air quality objectively and quantitatively, analyze pollutant sources, and identify the effects of meteorology on gaseous pollutant dispersion.

2. SO_2 concentration

During the APCL project, air quality data were collected from observational stations (St-1 through St-5) from October 1999 to April 2001 and from observational stations (St-6 through St-8) from August 2000 to April 2001. Red stars in Fig. 2b mark the locations of observational stations where

Table 1
Air quality standards for annual and daily mean SO_2 concentrations (mg m^{-3}) used by the Chinese National Environmental Protection Agency

Level of criterion	Annual	Daily
1	0.02	0.05
2	0.06	0.15
3	0.10	0.25

daily SO_2 concentrations were calculated. Table 2 shows the geography of the stations and the temporal averages of SO_2 concentration in 2000 (January–December for St-1 to St-5 and August–December for St-6 to St-8). Station-5 (Yuzhong) is located in a clean countryside and was identified as the reference station, where the annual mean SO_2 concentration was less than the first-level national air quality criteria (comparison between Tables 2 and 1). Data from routine air quality observations including daily SO_2 concentrations were collected continuously by SEPA in Lanzhou from June 2000 to May 2001 (background station, St-E, Fig. 1b). Annual mean SO_2 concentrations were collected and computed from surface meteorological stations. Station-E was near St-4.

Fig. 3 shows the temporal variation of daily mean SO_2 concentrations at four APCL stations (St-1, St-3, St-4, and St-7) to represent District I, District II, District III, and District IV, respectively. The horizontal dashed and solid lines are referred to as the second- and third-level criteria for daily mean concentrations (Table 1). The SO_2 concentrations at the four stations were lower than the second-level criterion (0.15 mg m^{-3}) from April to October (late spring, summer, and autumn) except for a few occasions. However, from December to January (winter) the SO_2 concentration often exceeded the second-level standard with a high-occurrence rate of 0.82 at St-1 (District I, metropolitan area) to a relatively low-occurrence rate of 0.25 at St-7 (District IV, mixed residential, small factories, and farming area) In addition, the SO_2 concentration sometimes exceeded the third-level standard (0.25 mg m^{-3}). High SO_2 concentrations in the winter were due largely to household heating. The maximum daily mean SO_2 concentration was 0.52 mg m^{-3} in December 2000 at St-1 (District I). In addition, the annual mean SO_2 concentration for St-1 (Table 2) was 0.08 mg m^{-3}, which also exceeded the second-level annual mean standard of 0.06 mg m^{-3}.

Pollution at St-4 (District III, heavily industrialized area) lasted much longer than at the other observational stations. From November to April, the SO_2 concentration exceeded the second- (third-) level standard with the percentage of occurrence of 51% (19%). Besides, concentrations sometimes exceeded the third-level criterion with a maximum of 0.40, 0.46, and 0.47 mg m^{-3} in December 1999, November 2000, and January 2001, respectively, as well as monthly means of 0.21, 0.22, and 0.20 mg m^{-3} in November 1999, December 1999, and November 2000, respectively. Annual mean SO_2 concentration at St-4 (Table 2) was 0.08 mg m^{-3}, larger than the second-level criterion (0.06 mg m^{-3}). Similarly, the daily mean SO_2 concentration at St-3 (District II) and St-7 (District IV) often exceeded the second-level criterion in December and January.

3. Air pollution index

The air pollution index (API), which connects to human health, is a quantitative measure for uniformly reporting air quality for different constituents. The State Environmental Protection Agency classifies air quality standards into 5 major

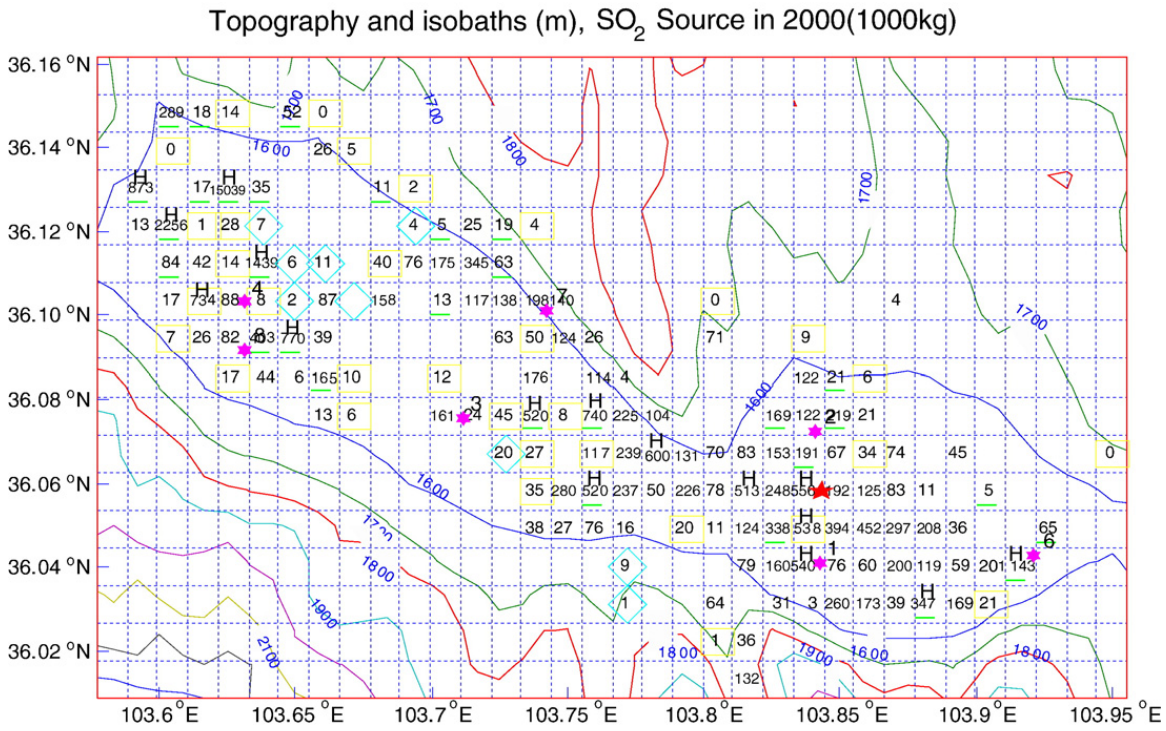

Fig. 2. Spatial distribution for annual SO_2 emissions per square kilometer (unit: 10^3 kg km^{-2}) in 2000. Here, the industrial sources are indicated with underlines; high-level sources are represented by the enclosed solid curves marked as "H". The dashed contours are topography (unit, m). (For interpretation of the references to color in this figure legend, the reader is referred to the web version of this article.)

Table 2
Location of observational stations and temporally total mean concentrations (mg m^{-3}) of SO_2 during the observational period

Ste	Longitude Ei	Latitude N	Height above surface (m)	Region	SO_2
St-1	103.84	36.04	25	Chengguan (District I)	0.08
St-2	103.84	36.07	11	Chengguan (District II)	0.03
St-3	103.71	36.08	15	Qilihe (District III)	0.05
St-4	103.63	36.10	22	Xigu (District II	0.08
St-5	104.09	35.84	4	Yuzhong County	0.01
St-6	103.92	36.04	19	Chengguan (District I)	0.02
St-7	103.74	36.10	15	Anning (District IV)	0.04
St-8	103.63	36.09	4	Xigu (District II)	0.06

Note that the second-level annual mean criterion is 0.06 mg m^{-3} for SO_2.

categories due to API values (Table 3): I (clean), II (good), III (low-level pollution), IV (mid-level pollution), and V (high-level pollution). Categories III and IV each have two sub-categories: III_1 and III_2 and IV_1 and IV_2, respectively. The API is calculated by first normalizing the measured concentrations

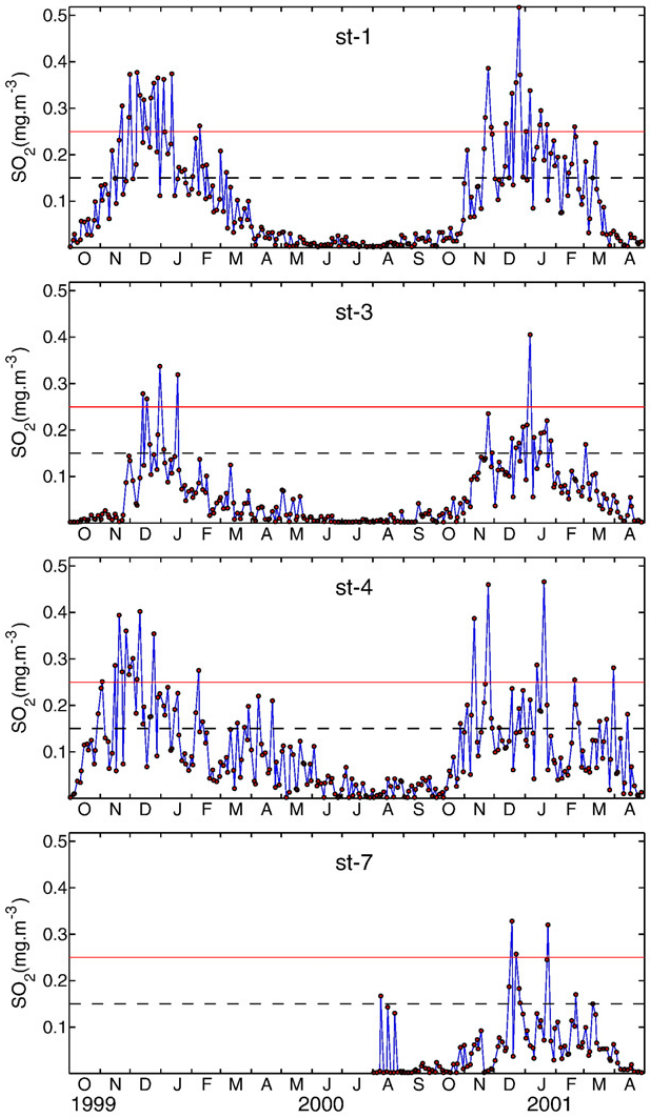

Fig. 3. Daily mean SO_2 concentrations (mg m^{-3}) at St-1, St-3, St-4, and St-7 representing four districts. Horizontal dashed line is the daily mean second-level criterion, while the horizontal solid line is the daily mean third-level criterion. Note that the daily mean SO_2 concentration shows strong seasonal variability with heavier pollution in the winter than in the summer.

Table 3
API and air quality management in China

Air pollution index	Air quality classification		Air quality description and management
API ≤ 50	I	Clean	No action is needed.
50 < API ≤ 100	II	Good	No action is needed.
100 < API ≤ 150	III_1	Low-level	People should be careful
150 < API ≤ 200	III_2	pollution	in outdoor activities.
200 < API ≤ 250	IV_1	Mid-level	People with existing heart
250 < API ≤ 300	IV_2	pollution	or respiratory illnesses are advised to reduce physical exertion and outdoor activities.
API ≥ 300	V	High-level pollution	Air pollution is severe. The general public is advised to reduce physical exertion and outdoor activities.

to a single scale. This normalization is based on different concentrations for the various pollutants, as chosen by SEPA. For SO_2, an API of 100, 200, or 300 corresponds to daily mean concentrations of 0.05, 0.15, or 0.25 mg m^{-3}, respectively.

The daily mean API for SO_2 averaged over all observational stations (Fig. 4) showed an evident seasonal variation with larger values (maximum around 200) in winter (low-level pollution, Category III) and much smaller values (usually smaller than 100) in other seasons. The monthly mean API for SO_2 showed similar seasonal variability with a larger value in winter and a much smaller value in other seasons. At the background station (St-E), the API for SO_2 was always less than 50 (data not shown here).

4. Numerical modeling

Meteorological effects on winter SO_2 pollution in Lanzhou were simulated using the coupled RAMS-HYPACT model.

4.1. RAMS

Non-hydrostatic RAMS 4.3 (Pielke et al., 1992) was used in the present study. The horizontal grid used a rotated, polar-stereographic projection. The vertical structure of the grid used a terrain-following coordinate system. The top of the model domain was flat, and the bottom followed the terrain (Tripoli and Cotton, 1982). The standard Arakawa C grid was used. RAMS contains many physics processes such as turbulent mixing (Helfand and Labraga, 1988), long- and short-wave radiation (Chen and Cotton, 1987), wet physics describing the interaction among the cloud formations and liquid, solid precipitation materials, sensible and latent heat exchanges between the atmosphere and multiple layers soil, surface vegetation and surface water, topographic dynamic affection, and cumulus convection parameterization. In the numerical simulation, a flat bottom with an elevation of 1460 m was assumed. This numerical simulation indicated that the 850-hPa level was nearly at the land surface. See the RAMS website at http://www.rams.atmos.colostate.edu for more information.

4.2. HYPACT

HYPACT was developed to simulate the motion of atmospheric tracers such as surface deposition, evaporation and

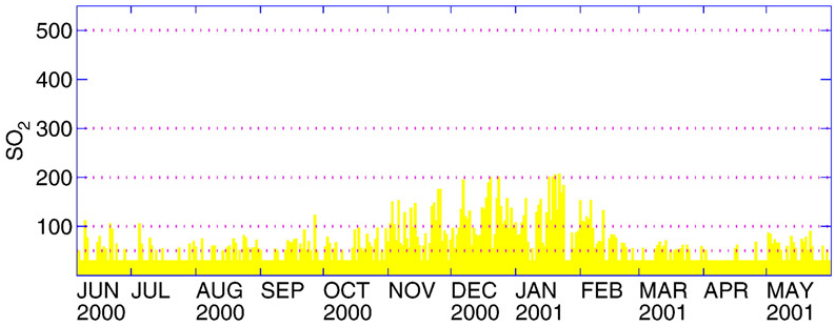

Fig. 4. API over all the observational stations.

condensation, precipitation scavenging, and other complex physical and chemical interactions influenced by winds and atmospheric turbulence (Walko et al., 2001). The HYPACT model adopted mixed Lagrangian and Eulerian approaches (Hurley and Physick, 1993). The Eulerian system in HYPACT was similar to RAMS where a scalar field was predicted with advection and diffusion. For small-scale, pollutant air masses during the initial state, the tiny-grid Lagrangian component represented sources of any size and maintained concentrated, narrow pollutant plumes until they were broadened by atmospheric dispersion. The position of a SO_2 plume is described by

$$\begin{aligned} X(t+\Delta t) &= X(t) + (u+u')\Delta t \\ Y(t+\Delta t) &= Y(t) + (v+v')\Delta t \\ Z(t+\Delta t) &= Z(t) + (w+w')\Delta t \end{aligned} \quad (1)$$

where u, v, and w are the three-dimensional, grid scale wind components and u', v', and w' are the three-dimensional, sub-grid scale (turbulence) wind components.

When the SO_2 plume became large enough to be recognized by the Eulerian system, the Eulerian method was used. The Lagrangian pollutant plume can be converted into a concentration field and then advected using an Eulerian formulation. The location and concentration of the SO_2 plume was predicted by HYPACT using meteorological output from RAMS. While a purely Eulerian treatment for the calculation of SO_2 concentration using RAMS was possible, the HYPACT module offered an alternative method for estimating atmospheric transport and dispersion that was not restricted by the spatial resolution of the RAMS model.

4.3. Boundary and initial conditions

On the ground surface, we used the U.S. Geological Survey vegetation 25-category with type-1 for urban/built-up land and type-4 for mixed dry/irrigational plants. The NCEP (U.S. National Weather Service, National Center for Environmental Predictions) data along the lateral boundary (every 6 h) of the largest box from December 1–31, 2000, was taken as the open boundary condition. One-way nesting was used for the triple-nested grid system. The larger model provided the lateral boundary conditions for the smaller model using a five-point buffer zone. The atmosphere was at rest ($V=0$) with horizontally uniform temperature and specific humidity soundings, which were taken from NECP re-analyzed data for Lanzhou at 0:00 GMT [0700 Beijing time (BT)] on December 1, 2000. RAMS was integrated from the initial conditions with the temporally varying solar irradiance at the top of the atmosphere since December 1, 2000.

Using the RAMS multiple grid-nested scheme (Table 4), model equations were solved simultaneously on any number

Table 4
Numerical features of the RAMS model

Nested grid	Center coordinate	Grid points	Grid interval	Time step
1st	103.8°E, 36.06°N	40×30	54 km	90 s
2nd	103.8°E, 36.06°N	38×29	18 km	30 s
3rd	103.8°E, 36.06°N	38×29	6 km	10 s
4th	103.8°E, 36.08°N	38×29	2 km	10/3 s
5th	103.8°E, 36.08°N	62×42	1 km	5/3 s

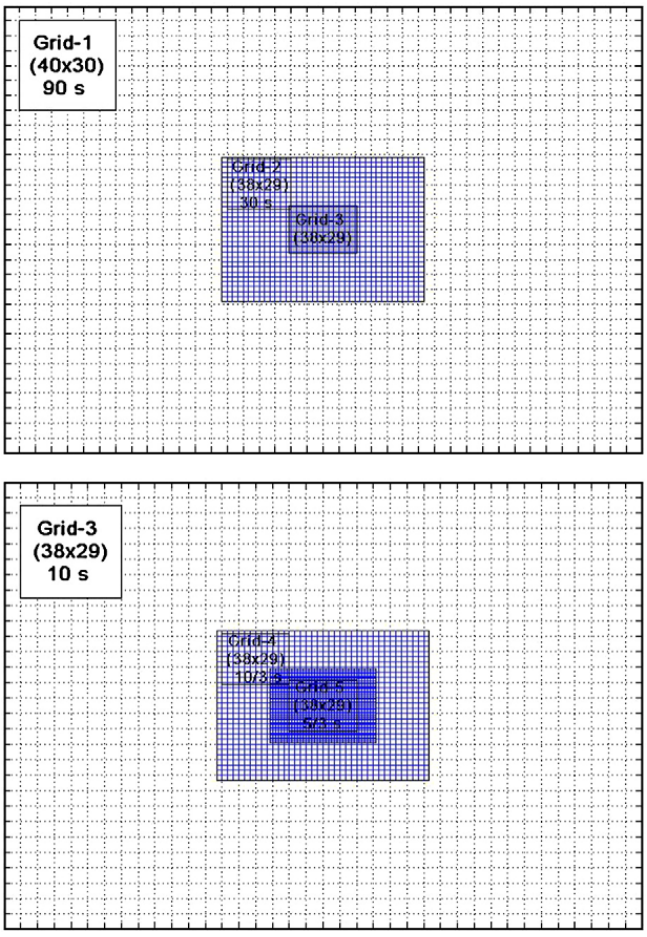

Fig. 5. Illustration of five nested grid systems. The last two grid systems (Grid-4 to Grid-5) are centered at (103.8°E, 36.08°N).

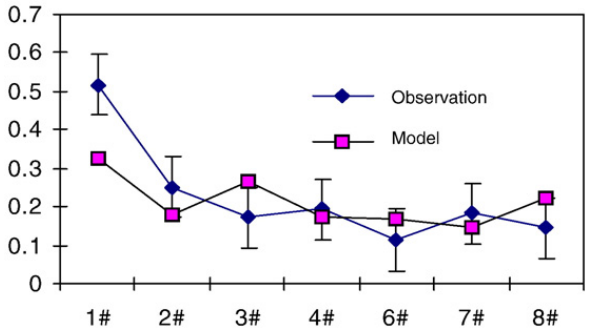

Fig. 6. Simulated and observed daily mean SO_2 concentration (mg/m^3) on December 12, 2000.

of interacting computational meshes of differing spatial resolution. The time-dependent model solution was first updated on the coarsest grid. A tri-quadratic spatial interpolation was then performed to obtain values that were assigned to the spatial boundaries of a finer grid nested within a coarser grid. The model fields on the finer grid were then updated using the coarser grid interpolated values as the spatial boundary conditions. Once the finer grid was at the same time level as the coarser grid, local spatial averages of the fine grid fields were obtained and used to overlay the coarse grid fields. The two-way interaction between the nested grids was performed following the scheme by Clark and Hall (1991) and Walko et al. (1995).

Five nested grids and 25 vertical levels illustrated by Chu et al. (2005) were used (Fig. 5). The vertical spacing was 200 m near the surface and increased to 800 m above 2400 m. The vertical grid structure was the same for all five nested grids. The outer grid (Grid-1) was a 40×30 grid with a horizontal resolution of 54 km and a time step of 90 s. The first nested grid (Grid-2) was a 38×29 grid with a horizontal resolution of 18 km and a time step of 30 s. The second nested grid (Grid-3) was a 38×29 grid with a horizontal resolution of 6 km and a time step of 10 s. The third nested grid (Grid-4) was a 38×29 grid with a horizontal resolution of 2 km and a time step of 10/3 s. The innermost grid (Grid-5) was a 38×29 grid with a horizontal resolution of 1 km and a time step of 5/3 s. The first three grid systems (Grid-1 to Grid-3) were centered at (103.8°E, 36.06°N). The last two grid systems (Grid-4 and Grid-5) were centered at (103.8°E, 36.08°N). After integrating RAMS, meteorological variables were inputted to HYPACT every hour.

4.4. Sulfur dioxide pollution sources

Pollution sources can be flexibly set in HYPACT as single or multiple, instantaneous, continuous, or time-varying. The source geometry can be point, line, area, or volume with various orientations, based on the spatial dimensions and the horizontal section shape of the actual sources of pollution. The SO_2 sources were divided into two types: the industrial type with weak seasonal variability and the residential type with strong seasonal variability (larger emission in winter than in summer due to heating). The chimney height varied with the HYPACT grid cell (1×1 km). For any grid cell, the pollution source was considered as the point source with a 30-m stack height if (a) at least one chimney in the grid cell was higher than or equal to 30 m (more likely for industrial sources) and (b) the pollution source was considered as the

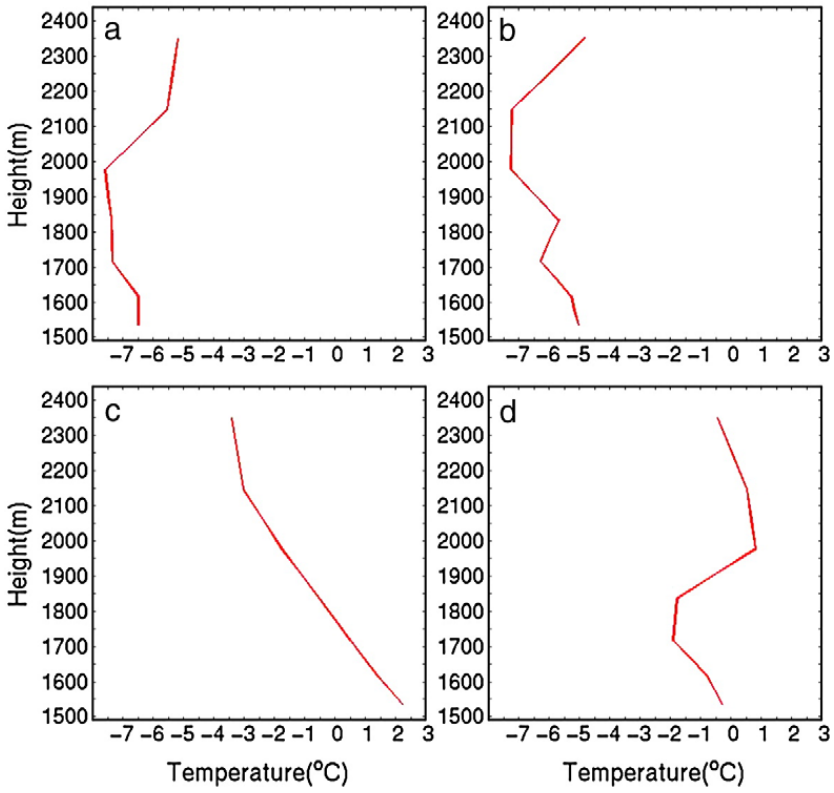

Fig. 7. Model simulated and horizontally averaged temperature profiles over the Grid-5 region (i.e., Lanzhou) on December 12, 2000: (a) 0200 BT, (b) 0600 BT, (c) 1700 BT (3 h after local noontime), and (d) 2100 BT.

area source with a 5-m stack height if no other chimney in the grid cell was higher than or equal to 30 m (more likely residential sources). Since only the total SO_2 emitted in 2000, $A(x, y)$, was available (see Fig. 2), the SO_2 emission rate for the point sources (F_p) was calculated by

$$F_p = \frac{A \times 10^{12}}{T \times 24 \times 3600} \quad (\text{unit}: \ \mu g \cdot s^{-1})$$

and the emission rate for the area sources (F_a) was computed by

$$F_a = \frac{A \times 10^{12}}{T \times 24 \times 3600 \times 10^6} \quad (\text{unit}: \ \mu g \cdot s^{-1} \cdot m^{-2})$$

Here, T is a total day of SO_2 emission during the year. In the present study, T equals 366 for industrial sources, and T equals 151 (around 5 months) for residential sources. Since the emission rate from residential sources depended on heating days, the estimated F_a may be large for a long, cold winter (real T>151 days) and vice versa.

4.5. Model verification

The daily mean SO_2 concentration predicted by the RAMS-HYPACT model has been compared with the APCL data as the relative root mean square error (i.e., the root mean square error divided by the observed mean SO_2 concentration) calculated for the period. This relative root mean square error of the predicted daily mean SO_2 concentration was around 8–15% from station to station. To demonstrate the capability of the RAMS-HYPACT model to predict severe SO_2 pollution events, the daily mean SO_2 concentration predicted by the model was compared to the observed daily mean SO_2 concentration within a range (between maximum and minimum) from the eight stations on December 12, 2000 (Fig. 6). The values predicted by the model were within the observational ranges at all stations except St-1 (residential district), where the value predicted by the model (0.32 mg/m^3) was smaller than the observed value (0.52 mg/m^3). Simulation results for the vertical SO_2 distribution were comparable with vertical pollutant profiles, which had been experimentally determined with tethered balloon soundings (e.g., Baumbach and Vogt 1995; Neu et al., 1994).

5. Atmospheric effects

The atmospheric static stability had seasonal and diurnal variability. With weak winds, the atmosphere was statically stable in evening and unstable in daytime. If the diurnal variability was filtered out, the atmosphere was statically stable in winter and unstable in summer. The connection between static stability and SO_2 concentration should have been similar for diurnal and seasonal variability. Thus, we analyzed the diurnal variations of static stability and SO_2 concentration simulated using the RAMS-HYPACT model to detect the effect of the atmospheric static stability. Fig. 7 shows a temporally varying sounding averaged horizontally over the innermost grid area (Grid-5) predicted by RAMS on December 12, 2002. Below the 2000-m height, the lapse rate ($\gamma = -\partial T/\partial z$) at night was 0.025 °C/100 m at 0200 BT, 0.05 °C/100 m at 0600 BT, and near 0 at 2100 BT (Fig. 7). The soundings showed evident inversion between 1700–1850 m

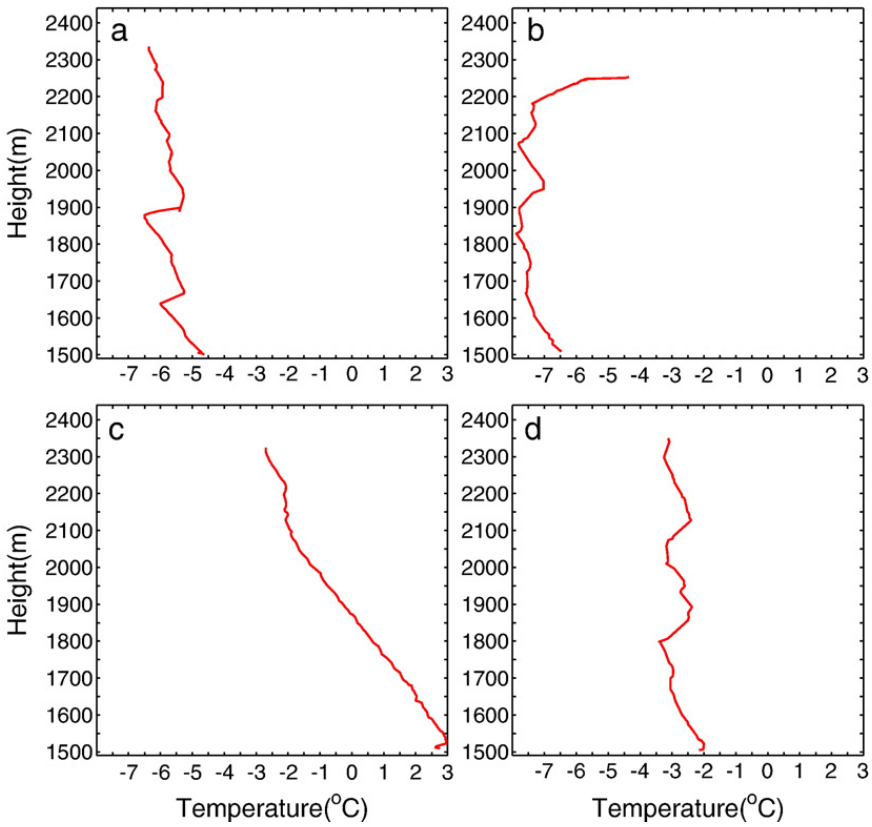

Fig. 8. Observed temperature profiles on December 12, 2000: (a) 0200 BT, (b) 0600 BT, (c) 1700 BT (3 h after local noontime), and (d) 2100 BT.

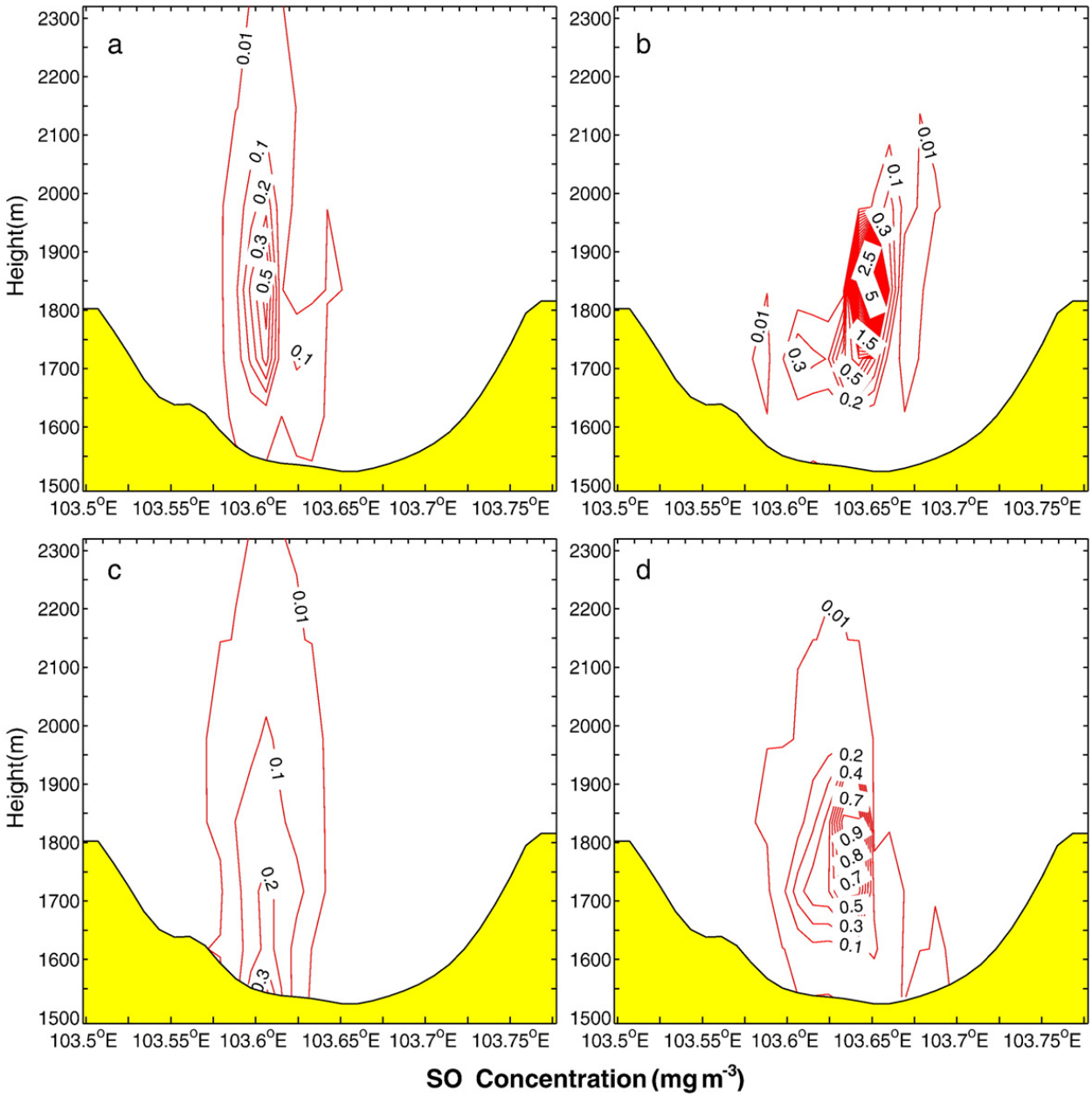

Fig. 9. Model simulated SO_2 concentration along 36.12°N on December 12, 2000: (a) 0200 BT, (b) 0600 BT, (c) 1700 BT (3 h after local noontime), and (d) 2100 BT.

at 0600 BT and between 1850–2000 m at 2100 BT. The daytime (1700 BT, three h after local noontime) sounding (Fig 7c) showed a linear lapse rate with the temperature decreasing from 2.2 °C at 1550 m to −3 °C at 2150 m (γ=0.87 °C/100 m). Since the dry-adiabatic lapse rate (Γ) was 0.98 °C/100 m, the simulated lapse rate in the air column 500–600 m above the ground was always stable (day and night) (i.e., $\gamma<\Gamma$). However, the static stability [proportional to ($\Gamma-\gamma$)] was strongest at 2100 BT and weakest at 1700 BT.

The model-predicted sounding agreed with the observed sounding (Fig. 8) reasonably well. Below the 2000-m height, the observed lapse rate in the evening was 0.18 °C/100 m at 0200 BT and near 0 at 0600 BT and 2100 BT with evident inversions. The daytime (1700 BT) observed sounding (Fig. 8c) showed a linear lapse rate with the temperature decreasing from 3 °C at 1550 m to −2 °C at 2150 m (γ=0.83 °C/100 m). Thus, the observed lapse rate in the air column 500–600 m above the ground was always stable (i.e., $\gamma<\Gamma$). Similar to the modeling results, the observed static stability was strongest at 2100 BT and weakest at 1700 BT.

The winter sounding showed two features: (a) stable stratification during day and night and (b) strong stability at night and weak stability during the day. These features made SO_2 pollution very difficult to diffuse at night. After building up during the evening, SO_2 concentrations should reach a maximum before dawn. Because the atmosphere became less stable in the daytime, the SO_2 concentration should have been minimal 2–3 h after local noontime. The model-predicted spatial distribution of the SO_2 concentration along 36.12°N (Fig. 9) has evident diurnal variation associated with diurnal variation in static stability: heavy SO_2 pollution at 0600 BT and light SO_2 pollution at 1700 BT.

6. Conclusions

A. Special topographic features of the Lanzhou metropolitan area (long, narrow valley) blocked air streams due to large frictional forces and caused weak winds. In the winter, occurrence of calm winds was nearly 80%. In the evening (occasionally even in daytime) a low-level inversion existed to inhibit turbulent diffusion and, in turn, to cause heavy SO_2 pollution. Close connection between static stability and SO_2 pollution at Lanzhou, China, in winter was simulated using the coupled RAMS-HYPACT model.

B. The SO_2 pollution largely depended on the emission source. Among the four districts, the SO_2 pollution was heavy in District I (commercial and residential area) and District III (heavy industrial area).

C. Sulfur dioxide concentration had evident seasonal variability. It was generally within the second-level criterion (<0.15 mg m^{-3}) in spring, summer, and fall but was much higher than the second-level criterion and sometimes reached mid-level pollution (API>200) in winter.

D. The winter sounding in Lanzhou, China, had two features: (1) stable stratification during day and night, and (2) strong nighttime stability with weak daytime stability. Because of these features, it was difficult for SO_2 pollutants to diffuse at night. After building up during the evening, the SO_2 concentration reached a maximum level before dawn. During the day, the atmosphere was less stable, and the SO_2 concentration reached a minimal level 2–3 h after local noontime.

Acknowledgments

This work was jointly supported by the National Natural Science Foundation of China, Major Programs No. 40305020, and the Naval Postgraduate School. The data for this study were provided by the program entitled, “Air Pollution and Control in Lanzhou,” which is jointly sponsored by the local government of Gansu Province and the Chinese Academy of Science.

References

Baumbach, G., Vogt, U., 1995. A tethered-balloon measurement system for the determination of the spatial and temporal distribution of air pollutants such as O_3, NO_2, VOC, particles and meteorological parameters. Eurotrac Newsletter, vol. 16, pp. 23–29.

Chen, C., Cotton, W.R., 1987. The physics of the marine stratocumulus-capped mixed layer. Bound.-Lay. Meteor. 25, 289–321.

Chu, P.C., Lu, S.H., Chen, Y.C., 2005. A numerical modeling study on desert oasis self-supporting mechanism. J. Hydrol. 312, 256–276.

Clark, T.L., Hall, W.D., 1991. Multi-domain simulations of the time dependent Navier–Stokes equations: benchmark error analysis of some nesting procedures. J. Comput. Phys. 92, 456–481.

Helfand, H.M., Labraga, J.C., 1988. Design of a non-singular level 2.5 second-order closure model for the prediction of atmospheric turbulence. J. Atmos. Sci. 45, 113–132.

Hurley, P.J., Physick, W.L., 1993. A skewed, homogeneous Lagrangian particle model for convective conditions. Atmos. Environ. 27A, 619–624.

Jiang, J.H., Chen, Y.C., Peng, X.D., Hu, F., et al., 2001. Contributions of industrial and residential sources to atmospheric SO_2 concentration in winter over Lanzhou. Plateau Meteorol. 20 (suppl.), 15–21 (in Chinese with English abstract).

Neu, U., Kunzle, T., Wanner, H., 1994. On the relation between ozone storage in the residual layer and daily variation in near-surface ozone concentration—a case study. Bound.-Lay. Meteorol. 69 (3), 221–247.

Pielke, R.A., Cotton, W.R., Walko, R.L., et al., 1992. A comprehensive meteorological modeling system—RAMS Meteor. Atmos. Phys. 49, 69–91.

Shang, K.Z., Da, C.Y., Fu, Y.Z., et al., 2001. Stable energy in Lanzhou and its effect on air pollution. Plateau Meteorol. 20 (1), 76–81 (in Chinese with English abstract).

Tripoli, G.J., Cotton, W.R., 1982. The Colorado State University three-dimensional cloud/mesoscale model—1982. Part I: general theoretical framework and sensitivity experiments. J. Rech. Atmos. 16, 185–219.

Walko, R.L., Tremback, C.J., Pielke, R.A., Cotton, W.R., 1995. An interactive nesting algorithm for stretched grids and variable nesting ratios. J. Appl. Meteorol. 34, 994–999.

Walko, R.L., Tremback, C.J., Bell, M.J., 2001. HYPACT Hybrid Particle and Concentration Transport Model, User's Guide. Mission Research Corporation, Fort Collins, CO.